



Development Characteristics and Finite Element Simulation of Fractures in Tight Oil Sandstone Reservoirs of Yanchang Formation in Western Ordos Basin

Shilin Wang¹, Hu Li^{1,2*}, Lifei Lin³ and Shuai Yin^{4*}

¹School of Geoscience and Technology, Southwest Petroleum University, Chengdu, China, ²Department of Railway Engineering, Sichuan College of Architectural Technology, Chengdu, China, ³Research Institute of Yanchang Petroleum (Group) Co., Ltd., Xi'an, China, ⁴College of Geosciences and Engineering, Xi'an Shiyou University, Xi'an, China

OPEN ACCESS

Edited by:

Wei Ju,
China University of Mining and
Technology, China

Reviewed by:

Zhonghu Wu,
Guizhou University, China
Bobo Li,
Guizhou University, China

*Correspondence:

Hu Li
lihu860628@126.com
Shuai Yin
speedysys@163.com

Specialty section:

This article was submitted to
Economic Geology,
a section of the journal
Frontiers in Earth Science

Received: 28 November 2021

Accepted: 15 December 2021

Published: 07 January 2022

Citation:

Wang S, Li H, Lin L and Yin S (2022)
Development Characteristics and
Finite Element Simulation of Fractures
in Tight Oil Sandstone Reservoirs of
Yanchang Formation in Western
Ordos Basin.
Front. Earth Sci. 9:823855.
doi: 10.3389/feart.2021.823855

Structural fractures have a significant control effect on the large-scale accumulation of hydrocarbons in the Yanchang Formation. Previous studies have affirmed the important role of fractures in hydrocarbon accumulations in strongly deformed zones. However, for low-amplitude structural areas, the degree of fracture development is relatively low, and their control on sweet spots of hydrocarbons has not yet formed a unified understanding. In this paper, taking the Upper Triassic Yanchang Formation in the western Ordos Basin as an example, the development characteristics, prediction method, and the distribution of fractures in tight sandstone reservoirs in low-amplitude structural areas have been systematically studied using a large number of cores, thin sections, paleomagnetism, FMI logging, acoustic emission, productivity data, and finite element method. The research results showed that the Yanchang Formation in the study area mainly develop high-angle and vertical fractures, which were formed by regional tectonic shearing. Fractures are mainly developed in the fine-grained and ultra-fine-grained sandstones of the distributary channel and estuary bar microfacies, while the fractures in the medium-grained sandstones of the distributary channel and the mudstones of the distributary bay are relatively underdeveloped. The core fractures and micro-fractures of the Yanchang Formation all have the regional distribution characteristics, and the fracture strikes are mainly between NE50° and NE 70°. Moreover, the finite element method was used to predict the fractures in the target layer, and the prediction results are consistent with the actual distribution results of the fractures. The coupling analysis of fractures and tight oil sandstone distribution showed that the existence of fractures provided conditions for the accumulation of hydrocarbons in the Yanchang Formation. The confluence and turning areas of the river channels were repeatedly scoured by river water, and the rocks were brittle and easy to form fractures. The thickness of the fractured sandstone in these areas is usually greater than 0.4 m. Moderately developed fracture zones are prone to form hydrocarbon accumulation “sweet spots,” and the fracture indexes of these areas are usually distributed between 0.8 and 1.2. However, when the fracture index exceeds 1.2, over-developed fractures are unfavorable for the accumulation of hydrocarbons.

Keywords: ordos basin, Yanchang formation, fracture, FMI imaging logging, finite element, low-amplitude structure

INTRODUCTION

The sweet spot prediction of fractured reservoirs is a hot spot in the current petroleum industry research (Borgia et al., 1996; Du and Yang, 2004; Barton et al., 2009; Cai, 2020; Cheng et al., 2020). Fractured reservoirs have strong heterogeneity, so traditional fracture evaluation methods face many challenges, such as the fine identifications of fractured segments and fracture sweet spots of tight reservoirs based on geophysical methods (Baecher, 1983; Bhatti et al., 2020; Chen, 2020; Fan et al., 2020a; Han et al., 2021; Liu et al., 2021a). At present, the conventional methods for identifying and evaluating reservoir fractures include core observations, conventional and imaging logging (Dowd et al., 2007; Casini et al., 2016; Li et al., 2019; Cao et al., 2020; Fan et al., 2020b; Liu et al., 2020a; Bukar et al., 2021). The cores obtained by drilling can be used to directly observe the development of underground fractures (Dcrshowitz and Einstein, 1988; Li et al., 2021; Yang et al., 2021; Xu and Gao, 2020; Nakaya and Nakamura, 2007; Dong et al., 2018; Hong et al., 2020; Liu et al., 2020b; Liu et al., 2021b). However, due to the impact of drilling and stress release, the core will crack after it was taken from the downhole to the ground, so it is necessary to identify the cause of the fractures on the core (Fan et al., 2018; Gao, 2019; Fan, 2020; Fu and Wang, 2020; Liu et al., 2020c; Liu et al., 2020d; Liu et al., 2021c). In addition, it is difficult to determine the original orientation of the fractures in the collected cores, while imaging logging overcomes this shortcoming (Gao, 2019; Liu et al., 2021c).

The collection cost of conventional logging data is much cheaper than other data, so it is widely used in reservoir exploration and evaluation (Jiang et al., 2017; Liu et al., 2019; Santosh and Feng, 2020; Yoshida and Santosh, 2020; He et al., 2021; Huang et al., 2021). However, the logging response is a comprehensive reflection of the various characteristics of the rock, and it is easily affected by factors such as fillings, mud, and dissolution (Mardia et al., 2007; Laubach et al., 2009; Sun et al., 2014; Hu et al., 2020; Li et al., 2020; Kang, 2021). Therefore, it is very difficult to directly use conventional logging curves to identify fractures. Imaging logging can intuitively provide the image information of the borehole wall, so it is currently the most effective fracture identification method (Sait and Matthew, 2013; Liu et al., 2017; Zhao et al., 2017; Peacock et al., 2018; Zhang et al., 2020; Li, 2021; Xue et al., 2021; Zhao et al., 2021; Gao, 2021). High-quality imaging logging data can provide information such as strike, dip, and opening of fractures. The information volume collected by imaging logging is large, so this type of logging method is time-consuming and expensive, and is only used by a few key wells (Liu et al., 2017; Li, 2021).

The finite element method is an effective technique widely used in the prediction of fracture distribution in tight reservoirs in recent years. The application of this technology is based on the established mechanical and mathematical models, and it is assumed that the deformation of the rock mass is the main reason for the rock mass ruptures (Murry, 1965; Mizoguchi and Ueta, 2013; Sebacher et al., 2017; Yin and Gao, 2019; Paiaman and Ghanbarian, 2021). For the Ordos Basin, the Mesozoic strata mainly developed low-amplitude structures,

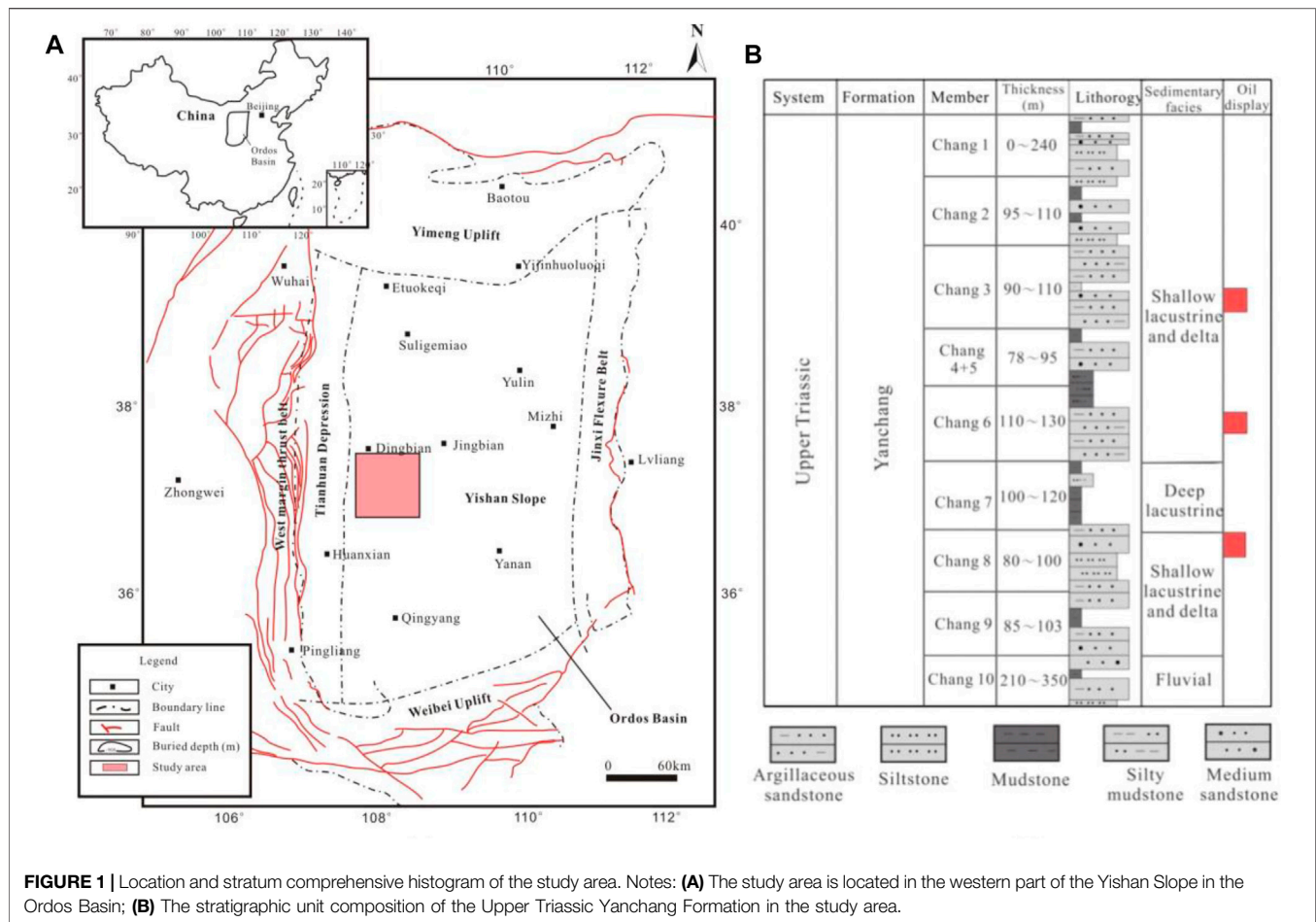
and low-amplitude structures represented weak compression stresses and weak deformation activities. Therefore, what kind of finite element model can be used to effectively characterize fractures is a problem worthy of in-depth study.

Tight oil sandstone reservoirs are developed in the Upper Triassic Yanchang Formation in the western Ordos Basin. The reservoir porosity is usually less than 10% and the gas permeability is less than 1 mD. The previous predictions of the sweet spots of tight oil sandstone reservoirs in the western Ordos Basin were mainly based on source rocks, sedimentary microfacies, diagenesis, and pore structures (Dong et al., 2018; Hong et al., 2020). There are few studies on the prediction of fractures in tightly heterogeneous continental tight sandstone reservoirs in low-amplitude structural areas. In this paper, taking the Upper Triassic Yanchang Formation in the western Ordos Basin as an example, the development characteristics, prediction method, and the distribution of fractures in tight oil sandstone reservoirs in low-amplitude structural areas have been systematically studied using a large number of cores, thin sections, paleomagnetism, FMI logging, acoustic emission, productivity data, and finite element method. This research can provide new ideas for the prediction of the “sweet spot” of continental tight oil sandstone reservoirs.

GEOLOGICAL BACKGROUND

The Ordos Basin is a large multi-cycle craton basin. According to the current structural morphology, the basin was divided into six primary structural units, including the Yimeng Uplift, Weibei Uplift, West Shanxi Flexfold Belt, Yishan Slope, Tianhuan Depression, and West Margin Thrust Structural Belt. Low-amplitude structures are developed in the marginal area of the basin, and the structural fluctuations per 1 km are usually less than 10 m. The study area is located in the western oil-bearing area of the Ordos Basin (Figure 1). The Chang 6 to Chang 8 oil-bearing intervals in the study area is developed on the west-dip monoclinical structure, and the scale of inherited low amplitude uplift is generally 1–4 km².

The sedimentary unit division of the study area is shown in Figure 1. The target layers are the Chang 6 and the Chang 8 Members of the Yanchang Formation. When the Chang 8 oil layer group was deposited, the lake basin had been in a sinking state until the Chang 7 oil layer group reached the maximum burial depth. At this time, the continental lake developed to the largest scale, and the deep lake source rock was formed at this stage. In the Chang 6 depositional period, the continental lake basin gradually began to shrink, and the subsidence rate was lower than the sedimentation compensation rate, and the lake basin delta formed. The Chang 6 and Chang 8 Members of the Yanchang Formation in the western oil region mainly develop underwater distributary channels, distributary bays, estuary bars, far sand bars, and semi-deep lake-deep lake mud microfacies. Chang 6 Member is further divided into Chang 6₁, Chang 6₂, Chang 6₃ and Chang 6₄ sub-members; and Chang 8 Member is further divided into Chang 8₁ and Chang 8₂ sub-members. Chang 6₁ and Chang 8₁ are the main oil producing horizons in this area.



METHODS

The technical methods used in this paper include conventional and FMI imaging logging, paleomagnetic experiments, acoustic emission testing, and finite element simulation. FMI imaging logging can provide high-resolution 360° omnidirectional two-dimensional petrophysical image information around the borehole wall (Ortega et al., 2006; Olson et al., 2009; Qie et al., 2021; Wang et al., 2021). The difference in resistivity or acoustic impedance caused by stratum characteristics such as lithology, fractures, pores, and bedding are converted into different color scales on the image. This technology intuitively and clearly displays the subtle changes in geological features such as the rock types, rock structures, sedimentary structures, pores, and fractures in the two-dimensional space surrounding the borehole wall in the form of images.

The 2G superconducting magnetometer measurement and the MMTD80 thermal demagnetizer from Magnetic Measurements were used for paleomagnetic experiments, and the fracture direction was determined. The demagnetization temperature of the samples include 12 points: normal temperature, 50°, 100°, 150°, 200°, 250°, 300°, 350°, 400°, 450°, 500°, and 600°. The remanence of the sample after demagnetization in each temperature range is measured, and the vector analysis is performed on the low-temperature viscous

remanence of the final period. Furthermore, the viscous remanence VRM of the modern geomagnetic field magnetization recorded by the core is obtained. Since the VRM direction is consistent with the modern geomagnetic field direction, that is, it is consistent with the geographic coordinates, the core fracture strike was obtained by referring to the core fracture mark line.

The main result of the acoustic emission test is to obtain the corresponding stress value when the rock specimen is cracked under the load. The rock specimen is subjected to an axial load, and then the acoustic emission signal generated during the entire compression process of the specimen is measured. The acoustic emission instrument used in this study is a rock physics testing system. The specimen will have several large ruptures during the process of axial load, and the load value corresponding to each rupture corresponds to the ancient stress value. In this study, the samples for acoustic emission testing were taken from the 2.213 m cores of Well D4578.

The main structural period stress intensities experienced by the target layer in the study area were simulated combined with the three-dimensional finite element method (Figure 2). The finite element simulation software was ANSYS. Based on core observations, FMI imaging logging fracture identifications and tectonic stress field simulations, the development characteristics and distribution of fractures in the tight reservoirs of the Yanchang Formation have been predicted.

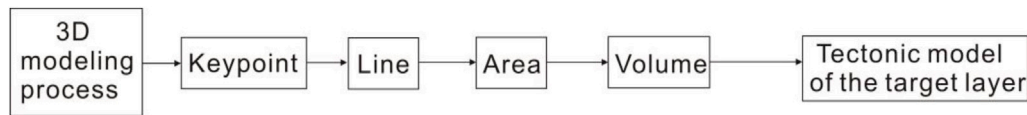


FIGURE 2 | Technical process of finite element simulation.

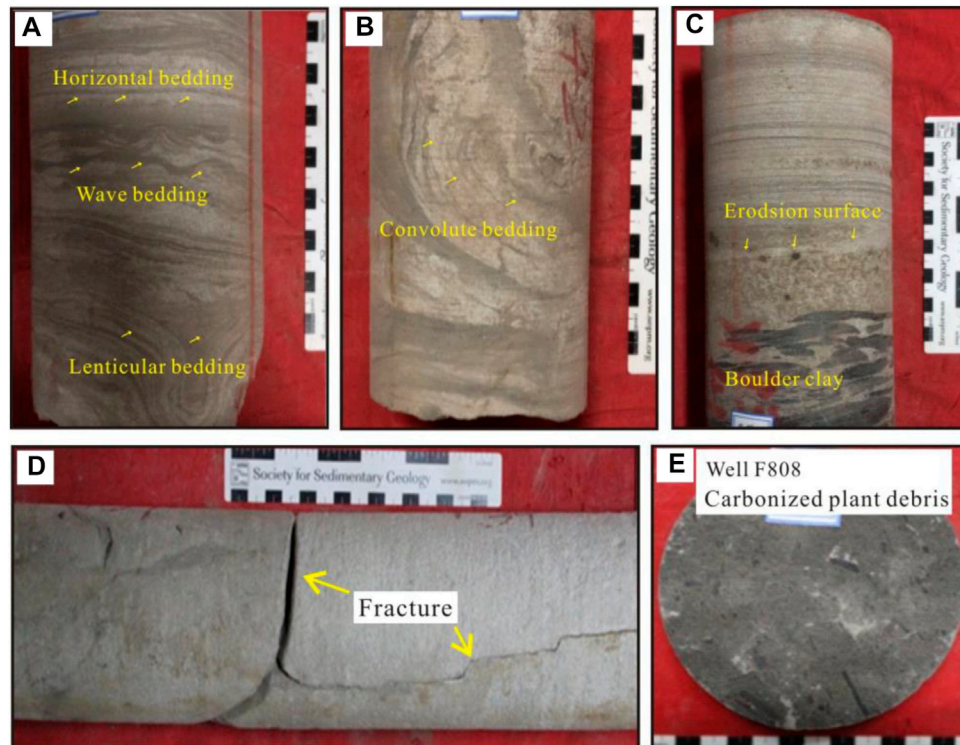


FIGURE 3 | Core pictures of the tight sandstone of Yanchang Formation in the study area. Notes: **(A)** Well J41, 1 707.87 m, bedding structures; **(B)** Well J41, 1 711.41 m, convolute bedding; **(C)** Well J41, 1 645.96 m, boulder clay; **(D)** Well F3, 1.074 m, vertical and horizontal fractures; **(E)** Well F808, 1 951.7 m, carbonized plant debris.

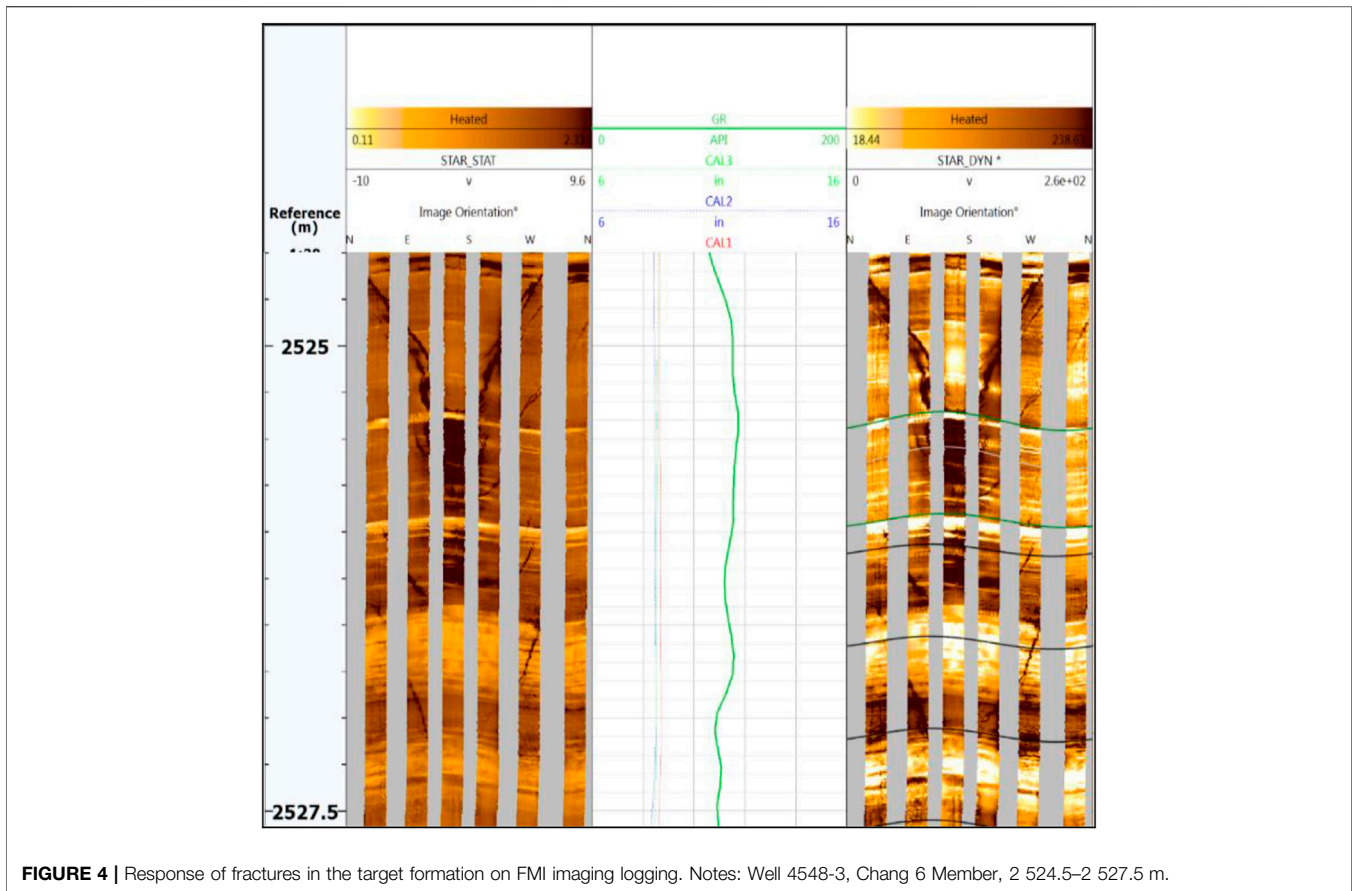
DEVELOPMENT CHARACTERISTICS OF FRACTURES IN TIGHT OIL SANDSTONE RESERVOIRS

Core Fractures

The sedimentary structures of a rock is a direct reflection of the sedimentary environment and hydrodynamic conditions when it was formed, and it has an inherent relationship with the rock combination (Robinson et al., 1998; Xu et al., 2006; Xu and Dowd., 2010; Zhang and Wang., 2020). Affected by changes in the depositional environment and hydrodynamic conditions, the sedimentary structures of the Chang 6 and Chang 8 Members include lenticular bedding, trough-like cross bedding, block bedding, wavy bedding, parallel bedding and erosion surfaces, and the convolute bedding can be seen locally (**Figures 3A–D**). They are all important signs for identifying sedimentary facies and microfacies (Yin et al.,

2019; Yin et al., 2020). Plant debris appeared in part of the cores (**Figure 3E**), and the color was gray-dark gray. The lithology of channel sand bodies was mainly medium-fine-grained sandstone (**Figure 3**).

The sandstone type in the study area is mainly feldspar sandstone, and feldspar is composed of potash feldspar and plagioclase. Among them, the plagioclase content is slightly higher than the potassium feldspar content, and the total feldspar content exceeds 50%. There is no significant difference between the Chang 6 and Chang 8 Members in the percentages of quartz, feldspar, and rock debris. The lithic components of the Chang 6 and Chang 8 Members are mainly eruptive rocks and granites, and the content of eruptive rocks is higher than that of granites. In addition, the main components of the cements of the Chang 6 and Chang 8 Members are carbonate minerals and clay minerals, while the content of clay iron, iron clay, and siliceous is very small.



The Yanchang Formation in the western oil region mainly developed high-angle and vertical fractures (Figure 3D). Most of the fracture surfaces observed in the core observations were straight and smooth, and the tail ends of the fractures had the phenomenon of folding tails, diamond-shaped knots, and diamond-shaped bifurcations. According to the core observations, the Yanchang Formation mainly developed vertical fractures, accounting for 70%, and oblique fractures and horizontal fractures accounted for 20 and 10%, respectively. Vertical and oblique fractures are mainly formed by regional structural shearing; and bedding fractures are mainly formed by the sliding of parallel bedding with peeling lineage under the combined action of sedimentary and tectonic stresses (Yin et al., 2018; Yin and Wu., 2020).

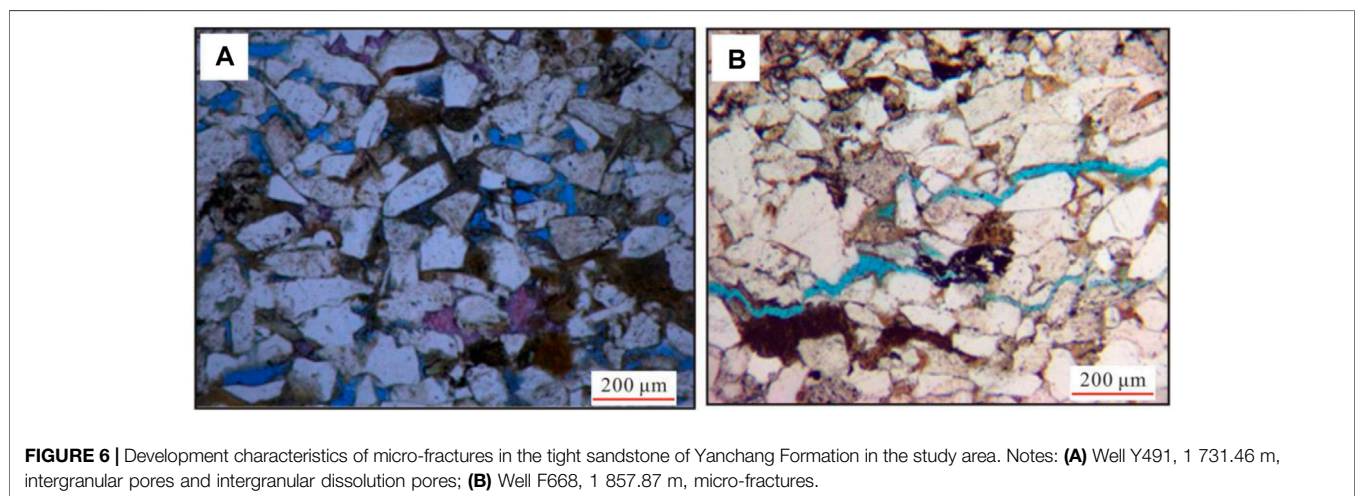
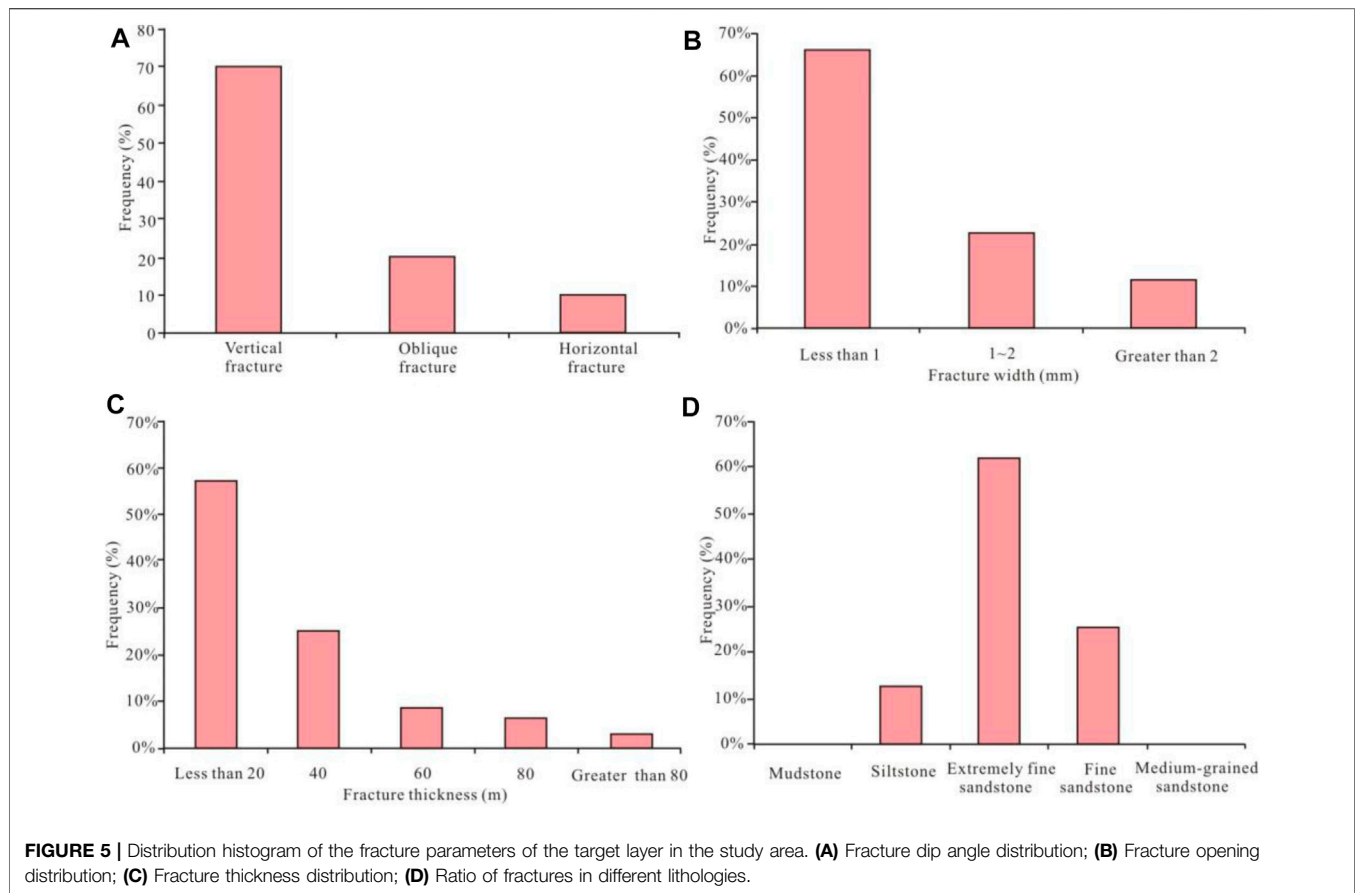
In addition to core observations, imaging logging can also help people visually observe the fractures (Yang et al., 2020; Zhao et al., 2020). Different types of fractures have different resistivity image characteristics. Under normal circumstances, when the fracture is in an open state, according to the fracture network invaded by the drilling fluid, the fracture exhibits an abnormal high conductivity. Furthermore, it is displayed as a dark sinusoidal curve on the electrical imaging and acoustic imaging diagrams. When the fracture angle is low, the amplitude of the sine curve is low, and when the fracture angle is high, the amplitude of the sine curve is high; vertical fractures appear as symmetrical dark

lines (Figure 4). When the fracture is half-filled or filled, the color of the sinusoidal curve displayed on the electrical imaging and acoustic imaging diagrams is different according to the difference of the filling degrees and the filling compositions.

The statistical results of the fracture parameters of the target layer in the study area are shown in Figure 5. The tight oil sandstone reservoir of the target layer mainly develops vertical fractures, and the fracture width is mostly less than 1 mm, and the vertical cut depth of the fracture is mostly less than 40 cm (Figures 5A–C). The statistical results also show that the fractures are mainly developed in the fine sandstone and ultra-fine sandstone of the distributary channel and estuary bar microfacies, while the fractures in the medium-grained sandstone of the distributary channel and the mudstone of the distributary bay are relatively underdeveloped.

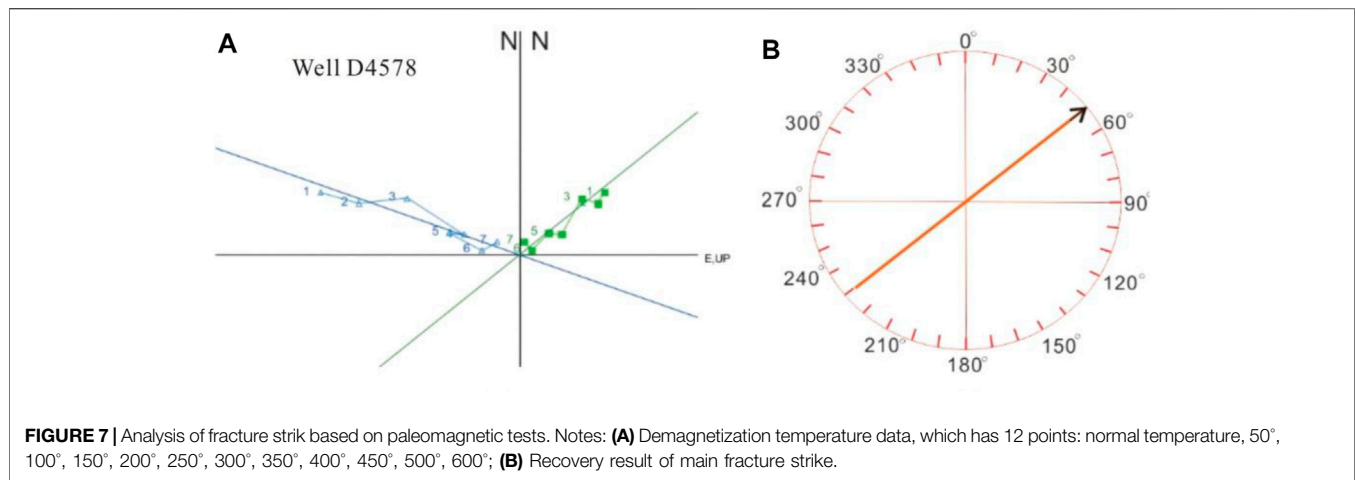
Microfractures

The Chang 6 and Chang 8 reservoirs of the Yanchang Formation in the study area have developed pores and micro-fractures. The pores are mainly intergranular pores (Figure 6A), followed by dissolution pores. The dissolution pores are mainly feldspar pores and a small amount of matrix pores. Both Chang 6 and Chang 8 reservoirs developed a large number of micro-fractures (Figure 6B). The volume of micro-fractures is very small, so its



storage performance is limited, and the micro-fractures mainly play the role of fluid drainage. Microscopic thin-section observations showed that most of the microfractures in the tight sandstone of the Yanchang Formation are open fractures, with good fracture effectiveness (**Figure 6B**); some of the microfractures were fully filled by mud and the fracture effectiveness was poor.

The microfractures in the Yanchang Formation are mostly straight fractures with a long extension distance and often pass through multiple particles. The previous divided the microfractures into Type I, Type II, and Type III (Laubach et al., 2009). Type I microfractures usually pass through a single particle or multiple particles with a small opening; Type II microfractures are usually distributed inside a single particle and are the results



of mutual extrusion between particles, with a large opening; Type III micro-fractures are inherited micro-fractures, which are mainly affected by diagenetic evolution. They have no fixed shape and are mainly distributed inside the particles. Observations of microfractures in the Yanchang Formation reservoir in the study area showed that the microfractures of the Yanchang Formation had the characteristics of regional fractures, which were Type I microfractures.

Fracture Strike

The paleomagnetic experiment results showed that the fracture strikes of the Yanchang Formation in the study area were mainly distributed between NE50° and NE70° (Figure 7), which further indicated that the direction of regional stress on these fractures was the NE direction (Yin et al., 2020). Under the action of the regional environmental stress in the NE direction, a group of symmetrical conjugate shear fractures will form in the formation (Yin et al., 2019). Therefore, the direction of the other group of conjugate fractures was biased toward the northwest direction. Of course, the degree of development and opening of the fractures in the NW direction are significantly lower than those in the NE direction.

FRACTURE PREDICTION BASED ON FINITE ELEMENT METHOD

Geological Model and Stress Loading

In this paper, ANSYS software was used for stress field simulation and fracture prediction (Yin et al., 2020). The main steps include modeling, element division, mechanical parameter assignment, stress loading, and fracture parameter calculation (Dong et al., 2018). The idea of the 3D geological model technology is based on the theoretical basis of shape function and trend surface analysis. The pre-processing module was used for geological model construction. In order to achieve the desired effect, the process is realized by a method based on spatial surface interpolation and fitting (Dong et al., 2018).

This modeling technique can realize the restoration of the tectonic stress field and the simulation of the spatial distribution

TABLE 1 | Meshing of the target layer in the study area.

Work area	Number of units	
	Nodes	Units
DL work area	63.218	275.446

of regional fractures. In the trend surface analysis method to restore the tectonic stress field, the dynamic mechanism of bumps or depressions is generally related to folds, and the tectonic stress system of bumps or depressions is consistent. The stress function solution can be obtained by solving the equation expressed by the surface deflection $W(x, y)$ in the elastic plane:

$$\frac{\partial^4 W}{\partial x^4} + 2 \frac{\partial^4 W}{\partial x^2 \partial y^2} + \frac{\partial^4 W}{\partial y^4} = \frac{q}{D}$$

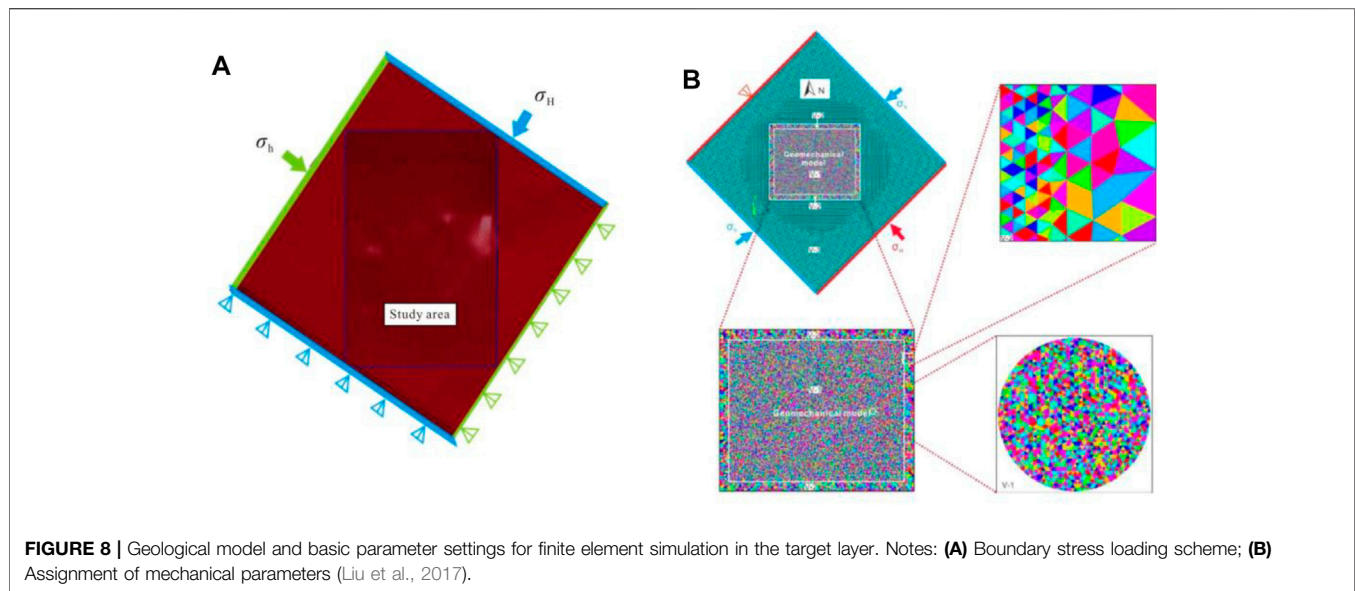
In the formula, $q(x, y)$ is the external load borne by the thin plate; D is the bending stiffness of the geological body, and its expression is as follows:

$$D = \frac{Eh^3}{12(1-\nu^2)}$$

In the formula: E and ν are the elastic modulus and Poisson's ratio, respectively; h is the thickness of the geological body.

The number of element nodes and units of the target layer finite element model based on the theoretical modeling of the shape function and the trend surface analysis method are shown in Table 1.

The boundary stress loading scheme and mechanical parameter assignment of the DL study area are shown in Figure 8. The fracture direction in the study area was mainly controlled by the stress in the NE direction. Combining regional stress and acoustic emission test results, the applied stress in the NE direction was 60 MPa, and the stress in the NW direction was 40 MPa. The grids were densified for the complex structures, such as the high points of the low-amplitude structure; while in the



relatively flat areas, the density of the grid was appropriately reduced. For the geological model shown in **Figure 8A**, the grid density was 20 m. The interpretation results of logging rock mechanics parameters were used to assign values to the grid cells and discrete modeling. The different colors in **Figure 8B** represented different rock mechanics parameter values.

In order to overcome the boundary effect and apply the boundary stress better, we expanded the periphery of the study area. When the boundary stress was applied, the overall displacement of the model was about 30 m. At this time, the displacement acting on a single finite element was also very small, so it can be ignored. The amount of strain was within the allowable range of deformation error, and the simulation results can be used for later fracture calculations.

The simulation results are mainly controlled by the geological model, environmental stress, and rock mechanical properties. These factors actually represent geological structure, stress expansion and sedimentary facies.

Paleo-Stress Calculation

The study area mainly managed two strong tectonic movements, namely, the Yanshan Movement squeezed in the NW direction and the Himalayan Movement squeezed in the NE direction (Yin and Wu., 2020). At present, NE-trending fractures are mainly developed in the study area. Therefore, the paleo-tectonic stress referred to in this study belongs to the Himalayan period. The samples of acoustic emission paleo-stress test were taken from the core of 2.213 m depth in well D4578 in the study area. The test results show that σ_H is 58.11 MPa and σ_h is 31.79 MPa. Furthermore, the calculation results of the paleostress of the target layer in the study area were compared with the measured results of acoustic emissions. The comparison results showed that the absolute error between the measured value and the predicted value of the horizontal maximum principal stress was 1.11 MPa; the absolute error between the measured value and

the predicted value of the minimum horizontal principal stress was -0.21 MPa. The paleo-stress simulation results were consistent with the measured results of acoustic emission, which proved that the calculation results of paleo-tectonic stress based on finite element were reliable.

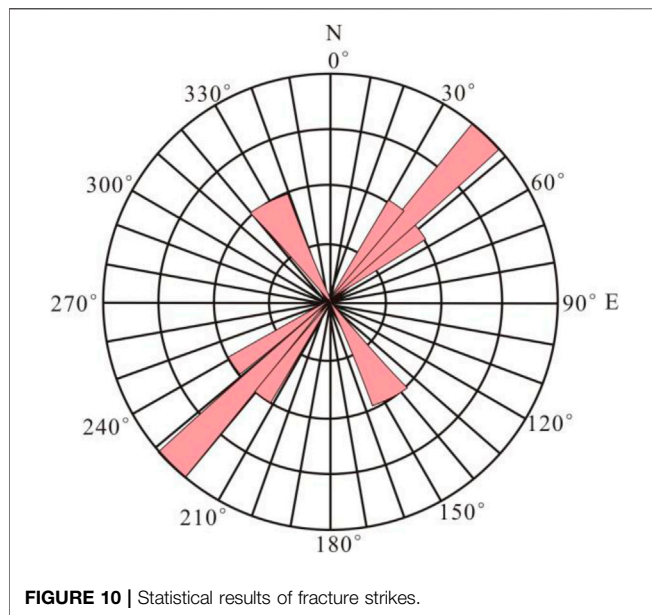
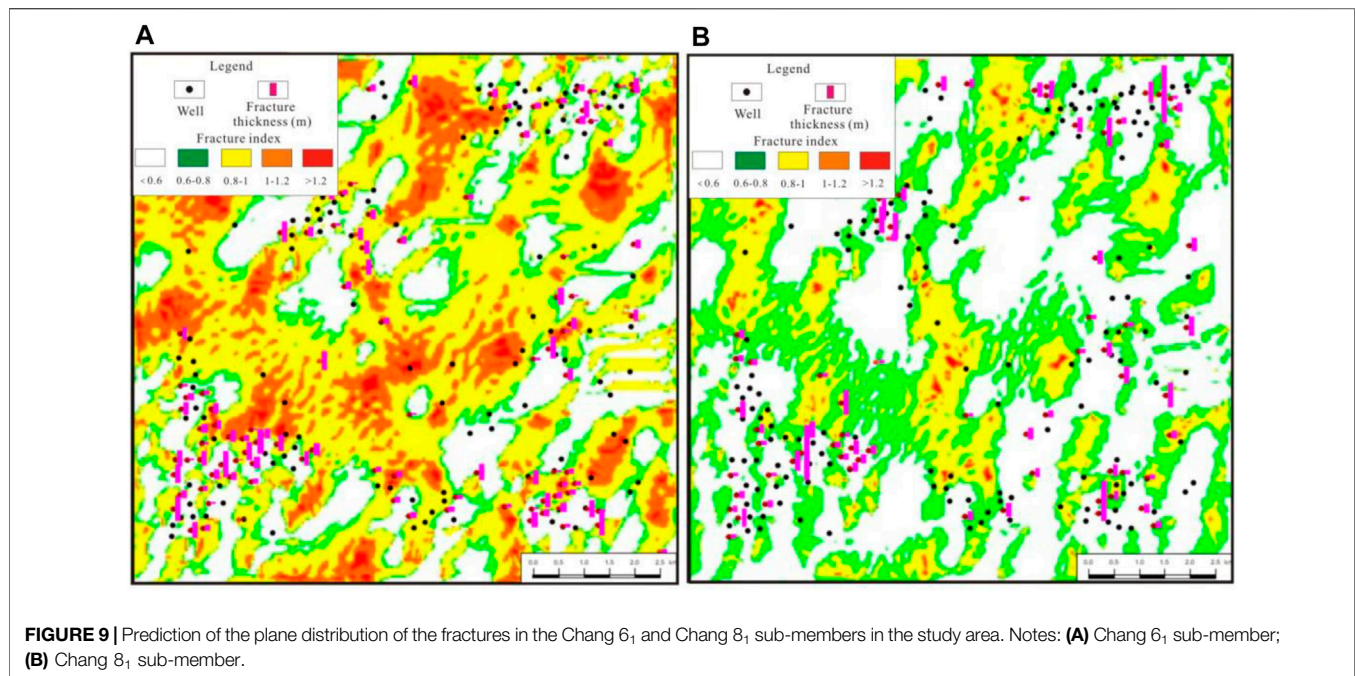
Prediction and Evaluation of Fracture Distribution

In this paper, a calculation model based on the principle of conservation of energy was used to predict the plane distribution of fractures in the target layer. The basic principle is that the existence of fractures can cause significant differences in the distribution of strain energy. The strain energy density method is an effective method to predict the micro-scale ruptures of rocks, so it is suitable for low-amplitude structural areas. For weakly deformed rock masses, according to the principle of conservation of energy, the work done by external force acting on the rock mass to deform it is equal to the strain energy of the rock mass. Furthermore, the work can be obtained by the displacement of a single element node on the acting force (Zhang et al., 2006; Zheng et al., 2020). The calculation formula of the fracture index U is as follows:

$$U = \frac{1}{2E} [(\sigma_x^2 + \sigma_y^2 + \sigma_z^2) - 2\nu(\sigma_x\sigma_y + \sigma_y\sigma_z + \sigma_z\sigma_x)] + \frac{2(1+\nu)(\tau_{xy}^2 + \tau_{yz}^2 + \tau_{zx}^2)}{2E}$$

In the formula, U is the fracture index; E is the Young's modulus; ν is the Poisson's ratio; σ_x , σ_y , and σ_z are the principal stresses in different directions; τ_{xy} , τ_{yz} , and τ_{zx} are the shear stress components in different stress directions.

The main oil layers in the study area are the Chang 6₁ and Chang 8₁ sub-members. Therefore, in this study, the Chang 6₁ and Chang 8₁ sub-members were used as the research object to



carry out fracture predictions. The coupling relationship between the fracture index and the fracture thickness of the Chang 6₁ and Chang 8₁ submembers is shown in **Figure 9**. The fracture thickness refers to the vertical thickness of the natural fracture segment. When the fracture index is greater than 1, it is considered that a core-scale fracture has occurred in the rock mass. The fracture index distribution is consistent with the fracture thickness results (**Figure 9**).

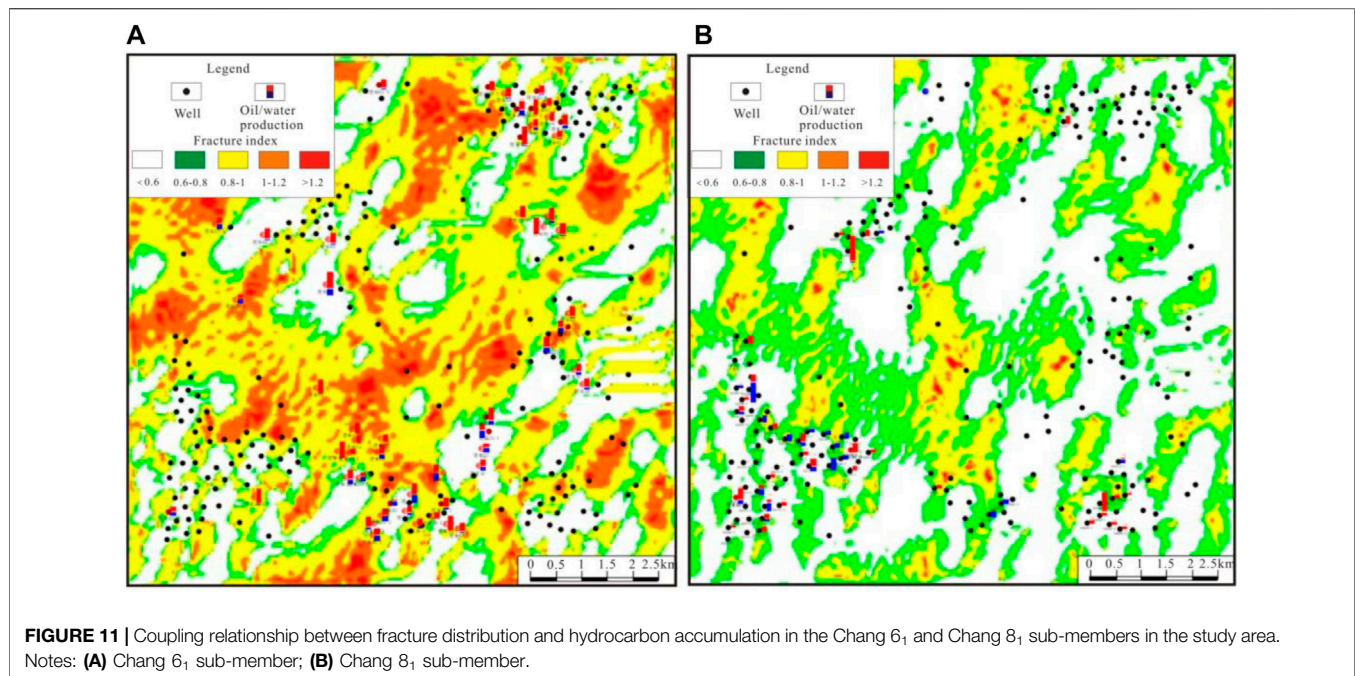
In addition, it can be seen from **Figure 9** that the predicted main direction of the fracture is between NE50° and 70°

(**Figure 10**), which is consistent with the paleomagnetic test results.

Coupling Analysis of Fracture Distribution and Hydrocarbon Accumulation

The Chang 6 and Chang 8 tight oil sandstone reservoirs of Yanchang Formation in the study area have no obvious oil-water interface, and lithological barriers form lithological traps. It is generally believed that the Chang 6 and Chang 8 oil layers in the study area have developed multi-stage channel sand bodies and mudstone superimposed vertically, forming a multi-stage effective lithological trap. Oil and gas fill and accumulate in multi-stage traps through high-permeability sandstone and fracture drainage system. Through this study, it is found that the widespread development of fractures is an important reason for the widespread oil-bearing in the longitudinal multi-layers of the Yanchang Formation in the study area. The provenance in the study area mainly came from the north, and the sand bodies are distributed along the north-south direction. The Chang 6 and Chang 8 members belong to the subfacies of the delta plain. Therefore, the river channel swung frequently, and the river in the confluence or turning areas were repeatedly scoured, and the sandstones were well sorted and had greater brittleness. Furthermore, the sand bodies in these locations were prone to rupture and form fractures under the conditions of tectonic activity (**Figure 11**). At present, the locations where oil reservoirs have been found are also mainly located in the confluence or turning areas of river channels, and the thickness of the fractured sandstone in these areas is usually greater than 0.4 m.

The scales of low-amplitude structural traps in the study area are relatively small, mainly distributed in 1–4 km². The



study found that fractures developed in the top and wing parts of the low-amplitude structures are relatively developed, and these areas are conducive to the large-scale accumulation of hydrocarbons. Regarding the relationship between the degree of fracture development and lithology, the fractures are mainly developed in the lithology of medium and low thickness fine-grained sandstone, and the thickness of the sand body is mainly distributed in the range of 5–15 m. For extremely thick sand bodies with thickness greater than 15 m, fractures are relatively underdeveloped. The study also found that the fractures mainly developed in the wings of the main channel. The middle part of the main channel has good physical properties, and the degree of fracture development is low. However, from the middle part of the river channel to the wing part, the grain size of the sand body becomes finer, and the compaction space of the rock particles gradually becomes smaller, and the fine-grained rock is more prone to rupture. In addition, the scale of fracture development is negatively related to the thickness of the sand body. Therefore, the thickness of the sand body in the channel wing is small, and the rock is prone to rupture.

It can also be found from **Figure 11** that there are many ranges of fracture index in the target layer of the study area greater than 1.2. Drilling cores also show that fractures in these areas are relatively developed. However, excessively developed fractures are not conducive to the enrichment of tight sandstone oil. This is because the sand and mudstones in the Yanchang Formation are frequently interbedded. When the fractures are developed too high, the fractures in the reservoir will communicate with the overburden and cause the escape of hydrocarbons.

On the whole, the formation and distribution of Yanchang Formation reservoirs are closely related to fracture distribution.

Moderately developed fracture zones are prone to form hydrocarbon accumulation “sweet spots,” and the fracture indexes of these areas are usually distributed between 0.8 and 1.2. When the fracture index exceeds 1.2, over-developed fractures are unfavorable to the formation of oil reservoirs. For the hydrocarbon drainage system, the fractures in the wings of the main sand body are more developed, which makes the sand body more likely to be preferentially charged by hydrocarbons. Due to the lack of fractures in the middle of the river channel, the superimposed high-permeability sand bodies are the main hydrocarbon drainage system.

CONCLUSION

- (1) The Yanchang Formation in the study area mainly develop high-angle and vertical fractures, which were formed by regional tectonic shearing. Fractures are mainly developed in the fine sandstone and ultra-fine sandstone of the distributary channel and estuary bar microfacies, while the fractures in the medium-grained sandstone of the distributary channel and the mudstone of the distributary bay are relatively underdeveloped.
- (2) The core fractures and micro-fractures of the Yanchang Formation all have the regional distribution characteristics, and the fracture strikes are mainly between NE50° and NE 70°.
- (3) The finite element method was used to predict the fractures in the target layer, and the prediction results are consistent with the actual distribution results of the fractures.
- (4) The coupling analysis of fractures and tight oil sandstone distribution showed that the existence of fractures provided conditions for the accumulation of hydrocarbons in the

Yanchang Formation. The confluence and turning areas of the river channels were repeatedly scoured by river water, and the rocks were brittle and easy to form fractures. The thickness of the fractured sandstone in these areas is usually greater than 0.4 m.

- (5) Moderately developed fracture zones are prone to form hydrocarbon accumulation “sweet spots,” and the fracture indexes of these areas are usually distributed between 0.8 and 1.2. However, when the fracture index exceeds 1.2, over-developed fractures are unfavorable for the accumulation of hydrocarbons.

REFERENCES

- Baecher, G. B. (1983). Statistical Analysis of Rock Mass Fracturing. *Math. Geology*. 15 (2), 329–348. doi:10.1007/bf01036074
- Barton, C., Moos, D., and Tezuka, K. (2009). Geomechanical Wellbore Imaging: Implications for Reservoir Fracture Permeability. *Bulletin* 93 (11), 1551–1569. doi:10.1306/06180909030
- Bhatti, A., Ismail, A., Raza, A., Gholami, R., Rezaee, R., Nagarajan, R., et al. (2020). Permeability Prediction Using Hydraulic Flow Units and Electrofacies Analysis. *Energy Geosci.* 1 (1–2), 81–91. doi:10.1016/j.engeos.2020.04.003
- Borgia, G. C., Bortolotti, V., Brancolini, A., Brown, R. J., and Fantazzini, P. (1996). Developments in Core Analysis by NMR Measurements. *Magn. Reson. Imaging* 14 (7–8), 751–760. doi:10.1016/s0730-725x(96)00160-9
- Bukar, M., Worden, R. H., Bukar, S., and Shell, P. (2021). Diagenesis and its Controls on Reservoir Quality of the Tambar Oil Field, Norwegian North Sea. *Energy Geosci.* 2 (1), 10–31. doi:10.1016/j.engeos.2020.07.002
- Cai, M. F. (2020). Key Theories and Technologies for Surrounding Rock Stability and Ground Control in Deep Mining. *J. Mining Strata Control. Eng.* 2 (3), 033037. doi:10.13532/j.jmsce.cn10-1638/td.20200506.001
- Cao, L., Yao, Y., Cui, C., and Sun, Q. (2020). Characteristics of *In-Situ* Stress and its Controls on Coalbed Methane Development in the southeastern Qinshui Basin, North China. *Energy Geosci.* 1 (1–2), 69–80. doi:10.1016/j.engeos.2020.05.003
- Casini, U., Hunt, D. W., Mosen, E., and Bounaim, A. (2016). Fracture Characterization and Modeling from Virtual Outcrops. *AAPG Bull.* 100 (1), 41–61. doi:10.1306/09141514228
- Chen, J. W. (2020). Analysis of Roadheader’s Rotary Table Onvibration Modal Based on Finite Element Method and Tested Data. *J. Mining Strata Control. Eng.* 2 (2), 026032. doi:10.13532/j.jmsce.cn10-1638/td.20191209.001
- Cheng, J. W., Zhao, G., Sa, Z. Y., Zheng, W. C., Wang, Y. G., and Liu, J. (2020). Overlying Strata Movement and Deformation Calculationprediction Models for Underground Coal Mines. *J. Mining Strata Control. Eng.* 2 (4), 043523. doi:10.13532/j.jmsce.cn10-1638/td.20200716.001
- Dcrshowitz, W. S., and Einstein, H. H. (1988). Characterizing Rock Joint Geometry with Joint System Models. *Rock Mech. Rock Eng.* 21 (1), 21–51.
- Dong, S., Zeng, L., Dowd, P., Xu, C., and Cao, H. (2018). A Fast Method for Fracture Intersection Detection in Discrete Fracture Networks. *Comput. Geotechnics* 98, 205–216. doi:10.1016/j.compgeo.2018.02.005
- Dowd, P. A., Xu, C., Mardia, K. V., and Fowell, R. J. (2007). A Comparison of Methods for the Stochastic Simulation of Rock Fractures. *Math. Geol.* 39 (7), 697–714. doi:10.1007/s11004-007-9116-6
- Du, Q. Z., and Yang, H. Z. (2004). Viscoelastic Wave Equations of Seismic Multi-Wave in Fractured media. *Acta Physica Sinica* 53 (8), 2802–2805. doi:10.7498/aps.53.2801
- Fan, C. H., He, S., Zhang, Y., Qin, Q. R., and Zhong, C. (2018). Development Phases and Mechanisms of Tectonic Fractures in the Longmaxi Formation Shale of the Dingshan Area in Southeast Sichuan Basin, China. *Acta Geologica Sinica* 92 (6), 2351–2366. doi:10.1111/1755-6724.13732
- Fan, C., Li, H., Qin, Q., He, S., and Zhong, C. (2020a). Geological Conditions and Exploration Potential of Shale Gas Reservoir in Wufeng and Longmaxi Formation of southeastern Sichuan Basin, China. *J. Pet. Sci. Eng.* 191, 107138. doi:10.1016/j.petrol.2020.107138
- Fan, C., Li, H., Zhao, S., Qin, Q., Fan, Y., Wu, J., et al. (2020b). Formation Stages and Evolution Patterns of Structural Fractures in marine Shale: Case Study of the Lower Silurian Longmaxi Formation in the Changning Area of the Southern Sichuan Basin, China. *Energy Fuels* 34 (8), 9524–9539. doi:10.1021/acs.energyfuels.0c01748
- Fan, K. (2020). Sudden Deformation Characteristic and Cutting Roof Support Technology for Double-Used Roadways in Longtan Mine. *J. Mining Strata Control. Eng.* 2 (3), 033032. doi:10.13532/j.jmsce.cn10-1638/td.20191227.001
- Fu, X., and Wang, R. F. (2020). Cooperative Self-Adaptive Control Model of Fluid Feeding System and Hydraulic Supports in Workingface. *J. Mining Strata Control. Eng.* 2 (3), 036031. doi:10.13532/j.jmsce.cn10-1638/td.20191203.001
- Gao, F. Q. (2019). Use of Numerical Modeling for Analyzing Rockmechanic Problems in Underground Coal Mine Practices. *J. Mining Strata Control. Eng.* 1 (1), 013004. doi:10.13532/j.jmsce.cn10-1638/td.2019.02.009
- Gao, F. Q. (2021). Influence of Hydraulic Fracturing of Strong Roof on Mining-Induced Stress Insight from Numerical Simulation. *J. Min. Strata Cont. Eng.* 3 (2), 023032–46. doi:10.13532/j.jmsce.cn10-1638/td.20210329.001
- Han, L., Shen, J., Qu, J., and Ji, C. (2021). Characteristics of a Multi-Scale Fracture Network and its Contributions to Flow Properties in Anthracite. *Energy Fuels* 35 (14), 11319–11332. doi:10.1021/acs.energyfuels.1c01465
- He, S., Li, H., Qin, Q., and Long, S. (2021). Influence of Mineral Compositions on Shale Pore Development of Longmaxi Formation in the Dingshan Area, Southeastern Sichuan Basin, China. *Energy Fuels* 35 (13), 10551–10561. doi:10.1021/acs.energyfuels.1c01026
- Hong, D., Cao, J., Wu, T., Dang, S., Hu, W., and Yao, S. (2020). Authigenic clay Minerals and Calcite Dissolution Influence Reservoir Quality in Tight Sandstones: Insights from the central Junggar Basin, NW China. *Energy Geosci.* 1 (1–2), 8–19. doi:10.1016/j.engeos.2020.03.001
- Hu, Q. F., Cui, X. M., Liu, W. K., Ma, T. J., and Geng, H. R. (2020). Law of Overburden and Surface Movement and Deformation Duetto Mining Super Thick Coalseam. *J. Mining Strata Control. Eng.* 2 (2), 023021. doi:10.13532/j.jmsce.cn10-1638/td.20191113.001
- Huang, F. R., Yan, S. X., Wang, X. L., Jiang, P. C., and Zhan, S. B. (2021). Experimental Study on Infrared Radiation Characteristics of Gneiss under Uniaxial Compression. *J. Mining Strata Control. Eng.* 3 (1), 013011. doi:10.13532/j.jmsce.cn10-1638/td.20200730.001
- Jiang, T., Zhang, J., and Wu, H. (2017). Effects of Fractures on the Well Production in a Coalbed Methane Reservoir. *Arab J. Geosci.* 10 (22), 494. doi:10.1007/s12517-017-3283-7
- Kang, H. P. (2021). Temporal Scale Analysis on Coal Mining Andstrata Control Technologies. *J. Mining Strata Control. Eng.* 3 (1), 013538. doi:10.13532/j.jmsce.cn10-1638/td.20200814.001
- Laubach, S. E., Olson, J. E., and Gross, M. R. (2009). Mechanical and Fracture Stratigraphy. *Bulletin* 93, 1413–1426. doi:10.1306/07270909094
- Li, H., Qin, Q., Zhang, B., Ge, X., Hu, X., Fan, C., et al. (2020). Tectonic Fracture Formation and Distribution in Ultradeep marine Carbonate Gas Reservoirs: A Case Study of the Maokou Formation in the Jiulongshan Gas Field, Sichuan Basin, Southwest China. *Energy Fuels* 34, 14132–14146. doi:10.1021/acs.energyfuels.0c03327
- Li, H., Tang, H., Qin, Q., Zhou, J., Qin, Z., Fan, C., et al. (2019). Characteristics, Formation Periods and Genetic Mechanisms of Tectonic Fractures in the Tight

DATA AVAILABILITY STATEMENT

The original contributions presented in the study are included in the article/supplementary material, further inquiries can be directed to the corresponding authors.

AUTHOR CONTRIBUTIONS

HL and SY are responsible for the idea and writing of this paper and SW and LL are responsible for the experiments and analysis.

- Gas Sandstones Reservoir: A Case Study of Xujiache Formation in YB Area, Sichuan Basin, China. *J. Pet. Sci. Eng.* 178, 723–735. doi:10.1016/j.petrol.2019.04.007
- Li, S. L., Liu, G. J., Jia, R. F., Xue, F., and Wang, K. Y. (2021). Study on Friction Effect and Damage Evolution of End Face in Uniaxial Compression Test. *J. Min. Strata Cont. Eng.* 3 (3), 033014. doi:10.13532/j.jmsce.cn10-1638/td.20210325.001
- Li, Y. (2021). Mechanics and Fracturing Techniques of Deep Shale from the Sichuan Basin, SW China. *Energ. Geosci.* 2 (1), 1–9. doi:10.1016/j.engeos.2020.06.002
- Liu, B., Bai, L., Chi, Y., Jia, R., Fu, X., and Yang, L. (2019). Geochemical Characterization and Quantitative Evaluation of Shale Oil Reservoir by Two-Dimensional Nuclear Magnetic Resonance and Quantitative Grain Fluorescence on Extract: A Case Study from the Qingshankou Formation in Southern Songliao Basin, Northeast China. *Mar. Pet. Geology.* 109, 561–573. doi:10.1016/j.marpetgeo.2019.06.046
- Liu, B., He, S., Meng, L., Fu, X., Gong, L., and Wang, H. (2021a). Sealing Mechanisms in Volcanic Faulted Reservoirs in Xujiaweizi Extension, Northern Songliao Basin, Northeastern China. *Bulletin* 105, 1721–1743. doi:10.1306/03122119048
- Liu, B., Sun, J., Zhang, Y., He, J., Fu, X., Yang, L., et al. (2021b). Reservoir Space and Enrichment Model of Shale Oil in the First Member of Cretaceous Qingshankou Formation in the Changling Sag, Southern Songliao Basin, NE China. *Pet. Exploration Dev.* 48 (3), 608–624. doi:10.1016/S1876-3804(21)60049-6
- Liu, B., Gao, Y., Liu, K., Liu, J., Ostadhassan, M., Wu, T., et al. (2021c). Pore Structure and Adsorption Hysteresis of the Middle Jurassic Xishanyao Shale Formation in the Southern Junggar Basin, Northwest China. *Energy Exploration & Exploitation* 39, 761–778. doi:10.1177/0144598720985136
- Liu, B., Yan, M., Sun, X., Bai, Y., Bai, L., and Fu, X. (2020a). Microscopic and Fractal Characterization of Organic Matter within Lacustrine Shale Reservoirs in the First Member of Cretaceous Qingshankou Formation, Songliao Basin, Northeast China. *J. Earth Sci.* 31, 1241–1250. doi:10.1007/s12583-020-1345-3
- Liu, B., Song, Y., Zhu, K., Su, P., Ye, X., and Zhao, W. (2020b). Mineralogy and Element Geochemistry of Salinized Lacustrine Organic-Rich Shale in the Middle Permian Santanghu Basin: Implications for Paleoenvironment, Provenance, Tectonic Setting and Shale Oil Potential. *Mar. Pet. Geology.* 120, 104569. doi:10.1016/j.marpetgeo.2020.104569
- Liu, B., Wang, S., Ke, X., Fu, X., Liu, X., Bai, Y., et al. (2020c). Mechanical Characteristics and Factors Controlling Brittleness of Organic-Rich continental Shales. *J. Pet. Sci. Eng.* 194, 107464. doi:10.1016/j.petrol.2020.107464
- Liu, B., Yang, Y., Li, J., Chi, Y., Li, J., and Fu, X. (2020d). Stress Sensitivity of Tight Reservoirs and its Effect on Oil Saturation: A Case Study of Lower Cretaceous Tight Clastic Reservoirs in the Hailar Basin, Northeast China. *J. Pet. Sci. Eng.* 184, 106484. doi:10.1016/j.petrol.2019.106484
- Liu, J., Ding, W., Yang, H., Wang, R., Yin, S., Li, A., et al. (2017). 3D Geomechanical Modeling and Numerical Simulation of *In-Situ* Stress fields in Shale Reservoirs: A Case Study of the Lower Cambrian Niutitang Formation in the Cen'gong Block, South China. *Tectonophysics* 712–713, 663–683. doi:10.1016/j.tecto.2017.06.030
- Mardia, K. V., Nyirongo, V. B., Walder, A. N., Xu, C., Dowd, P. A., Fowell, R. J., et al. (2007). Markov Chain Monte Carlo Implementation of Rock Fracture Modelling. *Math. Geol.* 39 (4), 355–381. doi:10.1007/s11004-007-9099-3
- Mirzaei-Paiaman, A., and Ghanbarian, B. (2021). A New Methodology for Grouping and Averaging Capillary Pressure Curves for Reservoir Models. *Energ. Geosci.* 2 (1), 52–62. doi:10.1016/j.engeos.2020.09.001
- Mizoguchi, K., and Ueta, K. (2013). Microfractures within the Fault Damage Zone Record the History of Fault Activity. *Geophys. Res. Lett.* 40 (8), 2023–2027. doi:10.1002/grl.50469
- Murry, G. H. (1965). Quantitative Fracture Study- Sanish Pool, McKenzie County, North Dakota. *Abstract AAPG Bull.* 49 (9), 1570–1571.
- Nakaya, S., and Nakamura, K. (2007). Percolation Conditions in Fractured Hard Rocks: A Numerical Approach Using The three Dimensional Binary Fractal Fracture Network (3D-BFFN) Model. *J. Geophys. Res.* 112 (B12), 1–15. doi:10.1029/2006jb004670
- Olson, J. E., laubach, S. E., and lander, R. H. (2009). Natural Fracture Characterization in Tight Gas Sandstones: Integrating Mechanics and Diagenesis. *Bulletin* 93 (11), 1535–1549. doi:10.1306/08110909100
- Ortega, O. J., Marrett, R. A., and Laubach, S. E. (2006). A Scale-independent Approach to Fracture Intensity and Average Spacing Measurement. *Bulletin* 90 (2), 193–208. doi:10.1306/082505050509
- Peacock, D. C. P., Sanderson, D. J., and Rotevatn, A. (2018). Relationships between Fractures. *J. Struct. Geology.* 106, 41–53. doi:10.1016/j.jsg.2017.11.010
- Qie, L., Shi, Y. N., and Liu, J. G. (2021). Experimental Study on Grouting Diffusion of Gangue Solid Filling Bulk Materials. *J. Mining Strata Control. Eng.* 3 (2), 023011. doi:10.13532/j.jmsce.cn10-1638/td.20210111.001
- Robinson, N. I., Sharp, J. M., Jr., and Kriscsl, I. (1998). Contaminant Transport in Sets of Parallel Finite Fractures with Fray Turc Skins. *J. Contaminant Hydrol.* 31 (1–2), 83–109. doi:10.1016/s0169-7722(97)00055-7
- Sait, B., and Matthew, J. P. (2013). Fault and Fracture Distribution within a tight-Gas sandstone Reservoir: Mesaverde Group, Mamm Creekfield, Piceance Basin, Colorado, USA. *Pet. Geosci.* 19, 203–222. doi:10.1144/petgeo2011-093
- Santosh, M., and Feng, Z. Q. (2020). New Horizons in Energy Geoscience. *Energ. Geosci.* 1 (1–2), A1. doi:10.1016/j.engeos.2020.05.005
- Sebacher, B., Hanea, R., and Stordal, A. S. (2017). An Adaptive Pluri-Gaussian Simulation Model for Geological Uncertainty Quantification. *J. Pet. Sci. Eng.* 158, 494–508. doi:10.1016/j.petrol.2017.08.038
- Sun, W., Li, Y. F., Fu, J. W., and Li, T. Y. (2014). Review of Fracture Identification with Well Logs and Seismic Data. *Prog. Geophys.* 29 (3), 1231–1242. doi:10.6038/pg20140332
- Wang, D. L., Hao, B. Y., and Liang, X. M. (2021). Slurry Diffusion of Singlefracture Based on Fluid-Solid Coupling. *J. Mining Strata Control. Eng.* 3 (1), 013038. doi:10.13532/j.jmsce.cn10-1638/td.20200429.001
- Xue, F., Liu, X. X., and Wang, T. Z. (2021). Research on Anchoring Effect of Jointed Rock Mass Based on 3D Printing and Digital Speckle Technology. *J. Mining Strata Control. Eng.* 3 (2), 023013. doi:10.13532/j.jmsce.cn10-1638/td.20210201.001
- Xu, N., and Gao, C. (2020). Study on the Special Rules of Surface Subsidence Affected by Normal Faults. *J. Min. Strata Cont. Eng.* 2 (1), 011007. doi:10.13532/j.jmsce.cn10-1638/td.2020.01.011
- Xu, C., and Dowd, P. (2010). A New Computer Code for Discrete Fracture Network Modelling. *Comput. Geosciences* 36 (3), 292–301. doi:10.1016/j.cageo.2009.05.012
- Xu, C., Dowd, P. A., Mardia, K. V., and Fowell, R. J. (2006). A Flexible True Plurigaussian Code for Spatial Facies Simulations. *Comput. Geosciences* 32 (10), 1629–1645. doi:10.1016/j.cageo.2006.03.002
- Yang, Li., Zhou, D-H., Wang, W-H., Jiang, T-X., and Xue, Z-J. (2020). Development of Unconventional Gas and Technologies Adopted in China. *Energ. Geosci.* 1 (1–2), 55–68. doi:10.1016/j.engeos.2020.04.004
- Yang, J. X., Luo, M. K., Zhang, X. W., Huang, N., and Hou, S. J. (2021). Mechanical Properties and Fatigue Damage Evolution of Granite Under Cyclic Loading and Unloading Conditions. *J. Min. Strata Cont. Eng.* 3 (3), 033016. doi:10.13532/j.jmsce.cn10-1638/td.20210510.001
- Yin, S., Dong, Li., Yang, X., and Wang, R. (2020). Experimental Investigation of the Petrophysical Properties, Minerals, Elements and Pore Structures in Tight Sandstones. *J. Nat. Gas Sci. Eng.* 76 (1), 1–14. doi:10.1016/j.jngse.2020.103189
- Yin, S., and Gao, Z. (2019). Numerical Study on the Prediction of "sweet Spots" in a Low Efficiency-Tight Gas sandstone Reservoir Based on a 3D Strain Energy Model. *IEEE Access* 7 (6), 1–12. doi:10.1109/access.2019.2933450
- Yin, S., Han, C., Wu, Z., and Li, Q. (2019). Developmental Characteristics, Influencing Factors and Prediction of Fractures for a Tight Gas sandstone in a Gentle Structural Area of the Ordos Basin, China. *J. Nat. Gas Sci. Eng.* 72 (12), 1–14. doi:10.1016/j.jngse.2019.103032
- Yin, S., Lv, D., and Ding, W. (2018). New Method for Assessing Microfracture Stress Sensitivity in Tight sandstone Reservoirs Based on Acoustic

- Experiments. *Int. J. Geomechanics* 18 (4), 1–10. doi:10.1061/(asce)gm.1943-5622.0001100
- Yin, S., and Wu, Z. (2020). Geomechanical Simulation of Low-Order Fracture of Tight sandstone. *Mar. Pet. Geology*. 100, 1–10. doi:10.1016/j.marpetgeo.2020.104359
- Yoshida, M., and Santosh, M. (2020). Energetics of the Solid Earth: An Integrated Perspective. *Energ. Geosci.* 1 (1–2), 28–35. doi:10.1016/j.engeos.2020.04.001
- Zhang, C., Song, W. D., Fu, J. X., Li, Y., and Zhang, K. C. (2020). Technology for Roadway Management of Fractured Rock Masses in a Submarine Gold Mine. *J. Mining Strata Control. Eng.* 2 (3), 033039. doi:10.13532/j.jmsce.cn10-1638/td.20200313.002
- Zhang, T., Switzer, P., and Journel, A. (2006). Filter-based Classification of Training Image Patterns for Spatial Simulation. *Math. Geol.* 38 (1), 63–80. doi:10.1007/s11004-005-9004-x
- Zhang, T., and Wang, Y. L. (2020). Study on Deformation Evolution Law and Support Technology of Surrounding Rock in Multiple Mining Roadway. *J. Mining Strata Control. Eng.* 2 (2), 023016. doi:10.13532/j.jmsce.cn10-1638/td.20200106.001
- Zhao, J. L., Liu, J. J., Zhang, Q. H., and Qu, X. R. (2017). Overview of Geophysical Exploration Methods and Technical of Tight sandstone Gas Reservoirs. *Prog. Geophys.* 32 (2), 840–848. doi:10.6038/pg20170253
- Zhao, Z., Wu, K., Fan, Y., Guo, J., Zeng, B., and Yue, W. (2020). An Optimization Model for Conductivity of Hydraulic Fracture Networks in the Longmaxi Shale, Sichuan basin, Southwest China. *Energ. Geosci.* 1 (1–2), 47–54. doi:10.1016/j.engeos.2020.05.001
- Zhao, K. K., Jiang, P. F., Feng, Y. J., Sun, X. D., Cheng, L. X., and Zheng, J. W. (2021). Investigation of the Characteristics of Hydraulic Fracture Initiation by Using Maximum Tangential Stress Criterion. *J. Min. Strata Cont. Eng.* 3 (2), 023520–46. doi:10.13532/j.jmsce.cn10-1638/td.20201217.001
- Zheng, H., Zhang, J., and Qi, Y. (2020). Geology and Geomechanics of Hydraulic Fracturing in the Marcellus Shale Gas Play and Their Potential Applications to the Fuling Shale Gas Development. *Energ. Geosci.* 1 (1–2), 36–46. doi:10.1016/j.engeos.2020.05.002

Conflict of Interest: Author LL was employed by the Research Institute of Yanchang Petroleum (Group) Co., Ltd.

The remaining authors declare that the research was conducted in the absence of any commercial or financial relationships that could be construed as a potential conflict of interest.

Publisher's Note: All claims expressed in this article are solely those of the authors and do not necessarily represent those of their affiliated organizations, or those of the publisher, the editors and the reviewers. Any product that may be evaluated in this article, or claim that may be made by its manufacturer, is not guaranteed or endorsed by the publisher.

Copyright © 2022 Wang, Li, Lin and Yin. This is an open-access article distributed under the terms of the Creative Commons Attribution License (CC BY). The use, distribution or reproduction in other forums is permitted, provided the original author(s) and the copyright owner(s) are credited and that the original publication in this journal is cited, in accordance with accepted academic practice. No use, distribution or reproduction is permitted which does not comply with these terms.